Applied Intelligence
https://doi.org/10.1007/s10489-020-02044-0

Multilinear subspace learning using handcrafted and deep features for face kinship verification in the wild

Mohcene Bessaoudi[1] · **Ammar Chouchane**[2] · **Abdelmalik Ouamane**[1] · **Elhocine Boutellaa**[3]

Accepted: 26 October 2020

Abstract

In this paper, we propose a new multilinear and multiview subspace learning method called Tensor Cross-view Quadratic Discriminant Analysis for face kinship verification in the wild. Most of the existing multilinear subspace learning methods straightforwardly focus on learning a single set of projection matrices, making it difficult to separate different classes. To address this issue, the proposed approach mutually learns multi-view representations for multidimensional cross-view matching. In order to decrease the effect of the within class variations for each mode of the tensor data, the proposed approach integrates the Within Class Covariance Normalization. Moreover, we propose a new tensor face descriptor based on the Gabor wavelets. Besides, we investigate the complementarity of handcrafted and deep face tensor features via their fusion at score level using the Logistic Regression method. Our extensive experiments demonstrate that the proposed kinship verification framework outperforms the state of the art, achieving 95.14%, 91.83% and 93.58% verification accuracies on Cornell KinFace, UB KinFace and TSKinFace face kinship datasets, respectively.

Keywords Kinship verification · Multilinear subspace learning · Multi-view representation · Tensors · local features · Hist-Gabor.

1 Introduction

Nowadays, automatic kinship verification from human face images is one of the most challenging research topics. The goal of kinship verification is to check the existence of a particular relationship between two individuals by visually comparing their facial appearances [5, 9, 12, 13, 46]. Checking human kin relationship based on faces is challenging because of the high level of appearance variability due to several effects such as hereditary contrast, gender distinction and age gap. There are numerous interesting real life applications for kinship verification such as family photographs organization, finding missing relatives, forestalling child trafficking, etc. Video surveillance and tracking systems are typical systems where the face-based family relationship checking can be deployed. In spite of the fact that a DNA test is the most exact approach for kinship verification [15], it lamentably cannot be utilized in several situations. Hence, face based kinship verification emerges as a potential alternative compared to the DNA.

Various computer vision approaches have been proposed to address the kinship verification challenge. Among the most viable literature works are learning-based methods such as metric learning [28], multi-metric learning [38], multilinear subspace learning [3]. Metric learning approaches have attained a satisfactory performance as demonstrated by [18, 21, 22, 24, 27, 28, 45]. These approaches are based on learning an appropriate discriminative metric depending on the provided data, which creates some restrictions. Additionally, such approaches neglect the complementary information, which can be provided by different features, resulting in weak performances when fusing these features. To overcome this limitations, other researches [16, 28, 29, 38], proposed the multi-metric learning approaches which learn multiple distance metrics for different types features at the same time. Nevertheless, multi-metric learning approaches cannot maintain the view specific properties and usually fail addressing the dilemma of the small sample size problem.

Recently, inspired by the significant achievement of multilinear subspace learning algorithms based on tensor

✉ Mohcene Bessaoudi
bessaoudi.mohcene@gmail.com

[1] Laboratory of LI3C, University of Biskra, Biskra, Algeria

[2] University of Yahia Fares Medea, Médéa, Algeria

[3] Telecommunication division, Centre de Développement des Technologies Avancées, Algiers, Algeria

Published online: 16 November 2020

modeling of data in different face analysis applications [2, 25, 26, 32, 39, 43], some researchers have been able to improve the kinship verification accuracy through the representation of face images as high order tensors and the application of multilinear subspace learning approaches. Examples of such approaches include Multilinear Side-Information based Discriminant Analysis [3] and Tensor Cross-view Quadratic Discriminant Analysis [17].

Motivated by the success of the multilinear analysis, our work presents a new tensor subspace learning method, Tensor Cross-view Quadratic Discriminant Analysis integrating the Within Class Covariance Normalization ($TXQDA_{WCCN}$), for tackling the problem of kinship verification in unconstrained environments. Specifically, a bunch of hybrid features, Hist-Gabor, Local phase quantization Binarized Statistical Image Features (LPQ+BSIf) and Visual Geometry Group (VGG) Face [34], are extracted from the face image. Each of these features provides a tensor representation of the face image. The proposed method $TXQDA_{WCCN}$ aims to project the face tensor representation into a new discriminative subspace, in which the margin of each face pair with a kin relation is reduced and that of each negative pair (no kin relation) is enlarged. To further enhance the kinship verification accuracies, we fuse the results from different types of features at score level.

The key contributions of the proposed framework for face based kinship verification with their motivations are the following:

1. We propose a new multilinear subspace approach for kinship verification, $TXQDA_{WCCN}$, based on multi-dimensional representation of face data. The kinship problem is modeled as a multilinear cross-view matching problem where the two face images of two different persons are seen as the two views of the kin relation. To reduce the class intra-variability impact, due to the big differences between the views, we apply WCCN.
2. We propose a new discriminative handcrafted face descriptor, Hist-Gabor, based on histograms of basic Gabor wavelets. To encode the face structure, the Gabor wavelets images are subdivided into several blocks. Taking advantage of the histogram features which considers the microstructures information such as plane area, spots and edges, the histograms of the face blocks concatenated, creating an enhanced feature vector.
3. Aiming to benefit from multiple face descriptors, we perform Logistic Regression (LR) score level fusion. This fusion scheme combines two handcrafted features, Hist-Gabor and (LPQ+BSIf), and a deep feature, VGG-Face, to exploit their complementarity. To the best of our knowledge, the proposed approach is the first one that takes the advantage of the discrimination power of three types of features for the kinship verification problem.

We extensively evaluate the proposed approach and compare it against the state-of-the-art methods on three challenging kinship databases, namely Cornell KinFace, UB KinFace and TSKinFace. Our method achieves high verification performances pointing out promising perspectives for our contributions.

The remainder of this paper is organized as follows. The proposed face kinship verification framework as well as the mathematical details of our algorithm are presented in Section 2. Experimental results on different databases and discussions are provided in Section 3. Finally, concluding remarks and future work are drawn in Section 4.

2 Proposed multilinear framework for kinship verification

In this section, we present the details of the proposed $TXQDA_{WCCN}$ for kinship verification based on multidimensional cross-view matching of pairs of facial images. As illustrated in Fig. 1. Our framework encompasses four important steps: feature extraction, multilinear subspace learning using $TXQDA_{WCCN}$, comparison (Cosine similarity) and LR score fusion. More information about each step is given below.

2.1 Feature extraction

Feature extraction is known to be one of the most crucial operations in face verification systems. The feature extraction step gives us with a feature vector or a feature matrix for each element in the database, which is considered to be the biometric signature of this element. In our system, two kinds, handcrafted and Deep, of well-established features are used. Regarding the handcrafted features, we use three methods, basic Gabor wavelets [7, 41], combination between the best two local descriptors [3, 17, 32] local phase quantization (LPQ) [31] and binarized statistical image feature (BSIf) [14] as well as our new feature extraction method named Hist-Gabor. For the Deep features, we utilize VGG-Face [34] network as feature extractor. The VGG-Face descriptor is a pre-trained face verification Convolutional Neural Network (CNN). VGG-Face is trained on over 2.6 million face images from 2622 different persons. Though the network is trained for identity verification, it has been successfully adopted as a generic face descriptor for many face analysis problems [4]. The input of the network is an RGB face image with size 224×224 pixels. Its layers are composed of a sequence of convolutional, pooling, and fully-Connected layers and followed by a Soft-Max layer. Each convolutional layer is followed by a relu activation function layer.

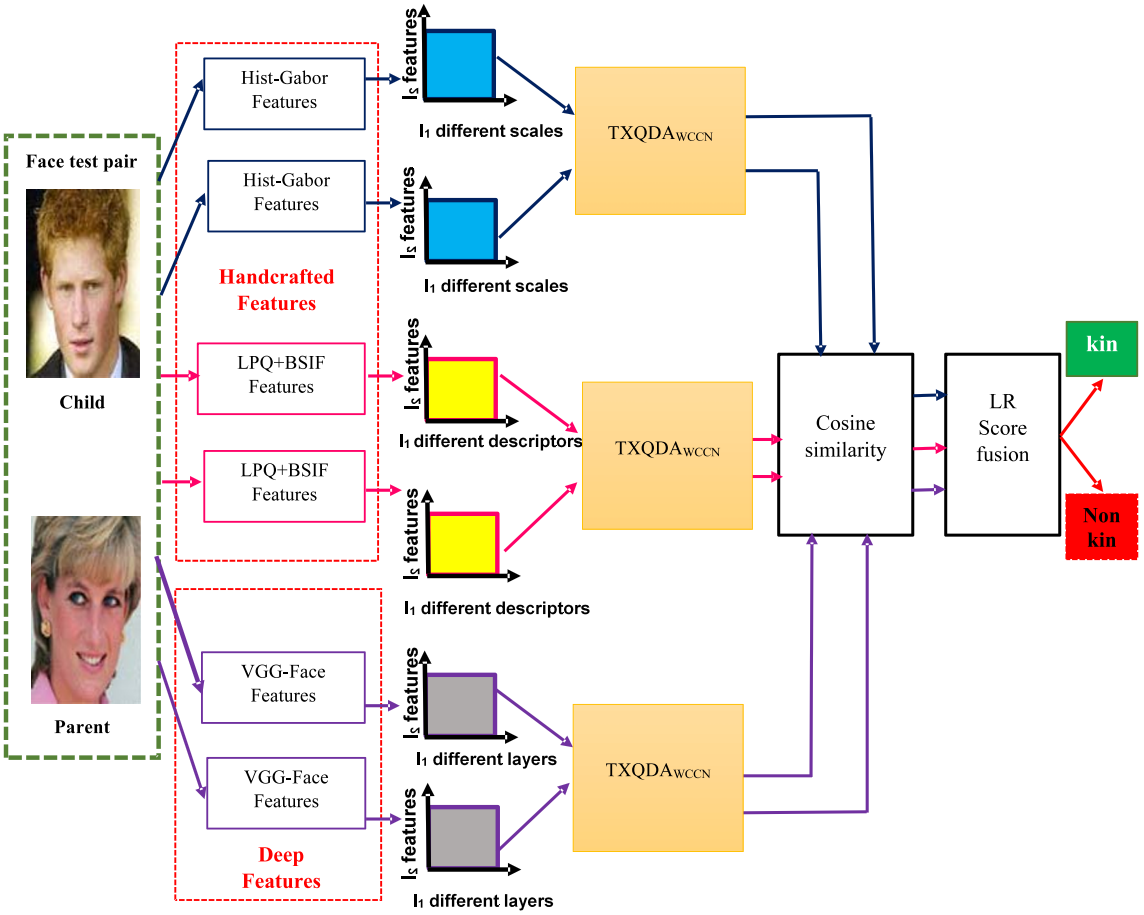

Fig. 1 The proposed pipeline for face kinship verification

2.1.1 Hist-Gabor face descriptor

The Gabor wavelets [19] is considered as one of the most widely used descriptors in the field of computer vision [40]. It is based on the application of a number of linear filters aiming to capture the image characteristics at different scales and orientations. Usually, the Gabor filter extracts the image frequency and spatial information from five scales (frequencies) and eight orientations (directions). The Gabor transformation is be obtained through the convolution between Gabor kernels G (a, b) and the input image I(x, y). Fig. 2 illustrates the result of the application of 40 Gabor filters, five scales and eight orientations, on a facial image [20]. The mathematical formulation of Gabor filter is as follow:

$$G(a,b) = \left(\frac{1}{2\pi\sigma_a\sigma_b}\right)\exp\left[-\frac{1}{2}\left(\frac{a^2}{\pi\sigma_a^2}+\frac{b^2}{\pi\sigma_b^2}\right) + 2\pi jW(z_0 a + y_0 b)\right] \quad (1)$$

where W represents the center frequency in the Fourier domain, (z_0, y_0) is the position of the Gabor filter. σ_a and σ_b are the variance of Gabor filter along a and b orientations, respectively.The multi-directionality and resolution can be acquired by rotating and scaling G(a, b):

$$G_{m,n}(a,b) = r^{-m}G(a',b') \quad (2)$$

where $\acute{a} = r^{-m}(a\cos\Theta + b\sin\Theta)$, $\acute{b} = r^{-m}(-a\sin\Theta + b\cos\Theta)$; r^{-m} represents the frequency factor, m=(0,1,...,S) denotes the scaling parameter, S represents the number of frequencies, $\Theta = n\pi/k$, and n(n = 1, 2,..., K) denotes direction parameter, K represents the number of directions. $G_{m,n}(a, b)$ is called Gabor wavelets.

The basic idea of the proposed Hist-Gabor is to represent the face image as depicted in Fig. 3. First, the input face image is convolved with the Gabor filter G(a,b) yielding the wavelets coefficients which describe the face texture at scale a and orientation b. The coefficients matrix is subdivided into k non-overlapping blocks, and each block is summarized into a histogram of 256 bins, then the histograms of different blocks are concatenated into a single vector, of size $k \times 256$, which describes the coefficients matrix. This process is applied to the result of each Gabor

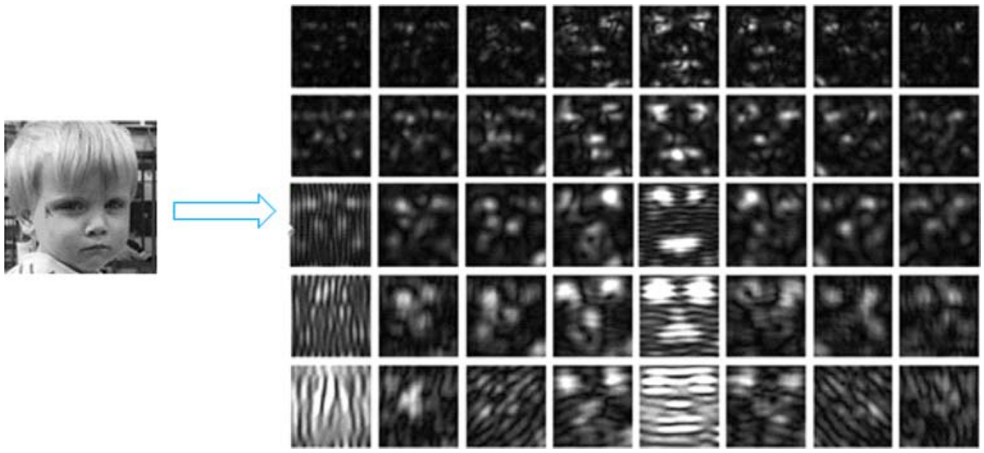

Fig. 2 Gabor wavelets decomposition of a face image using 5 frequencies and 8 orientations

filter yielding a × b feature vectors. Finally, these feature vectors are arranged in a matrix forming the new Hist-Gabor face image descriptor.

2.2 Proposed TXQDA$_{WCCN}$ multilinear subspace learning

For a better readability of the equations in this paper, we define a specific symbolic notation for different data types as described in Table 1.

Based on the these notations, the mathematical formulation of the proposed multilinear subspace learning is presented below.

TXQDA is considered as an extension of the linear XQDA [23] approach so that it works on high order tensors data. Thus, TXQDA seeks projecting the input tensors data to a new lower-dimensional subspace, where most the data variations in the original tensors is conserved. Let the cross-view training samples $\{\boldsymbol{A}, \boldsymbol{B}\}$ of c classes, represented as the mth-order tensors, where: $\boldsymbol{A} \in \mathbb{R}^{I_1 \times I_2 \times \cdots \times I_m \times x}$, comprises x samples of the first view (Parents) and $\boldsymbol{B} \in \mathbb{R}^{I_1 \times I_2 \times \cdots \times I_m \times y}$ comprises y samples of the second view (Children). TXQDA determines m interrelated projection matrices ($U_1 \in \mathbb{R}^{I_1 \times \acute{I}_1}$, $U_2 \in \mathbb{R}^{I_2 \times \acute{I}_2}$,..., $U_m \in \mathbb{R}^{I_m \times \acute{I}_m}$). Therefore, the objective function of XQDA [23] which corresponds to maximizing the covariance matrix V_I^k while minimizing the covariance matrix V_E^k in each mode of the training tensor:

$$J(U_k^*) = \text{argmax}_{U_K} \frac{Trace\left(U_k^T V_E^k U_k\right)}{Trace\left(U_k^T V_I^k U_k\right)} \tag{3}$$

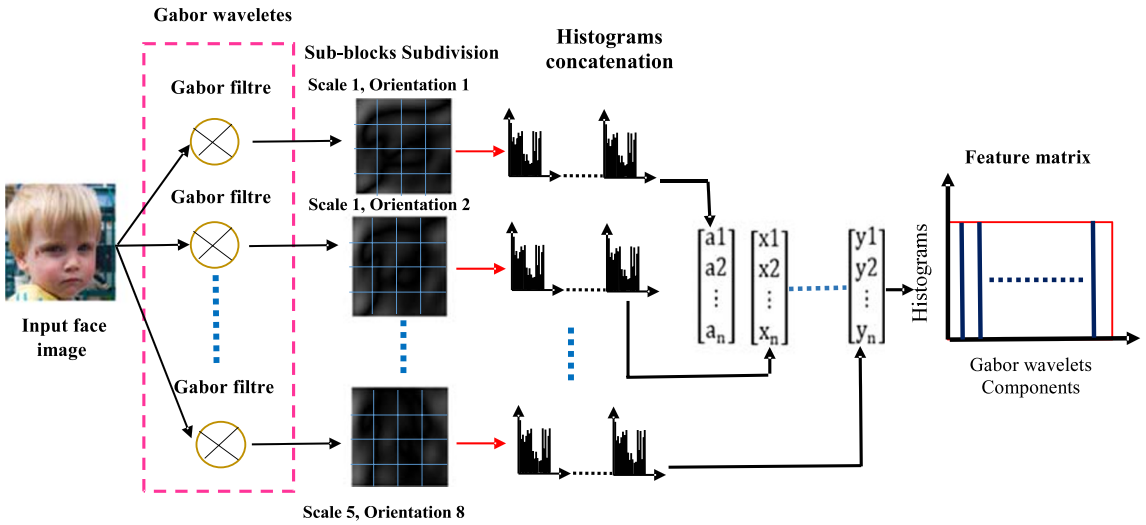

Fig. 3 Overview of the proposed Hist-Gabor face descriptor

Table 1 Respected notations

Notation	Description
Lowercase and uppercase symbols (eg. x, y, J, K)	Scalars
Bold lowercase symbols (eg. $\mathbf{x}$, $\mathbf{y}$)	Vectors
Italic uppercase symbols (eg. U, W)	Matrices
Bold italic uppercase symbols (eg. $\boldsymbol{X}$, $\boldsymbol{Y}$)	High order Tensors
$\boldsymbol{A} \in \mathbb{R}^{I_1 \times I_2 \times \cdots \times I_m}$	m^{th}-order tensor
I_m	Dimension of the m-mode
$\boldsymbol{A} \times_k U$	K-mode product

The two covariance matrices V_E^k and V_I^k for each k mode are computed using (4) and (10).

$$\begin{aligned} n_I V_I^k &= \sum_{p=1}^{\prod_{o \neq k} I_o} n_I V_I^{k,P}, n_I V_I^{k,P} \\ &= \widetilde{A}^{K,P} \left(\widetilde{A}^{K,P}\right)^T \widetilde{B}^{K,P} \left(\widetilde{B}^{K,P}\right)^T - M^{K,P} \left(F^{K,P}\right)^T \\ &\quad - F^{K,P} \left(M^{K,P}\right)^T \end{aligned} \tag{4}$$

where

$$\widetilde{A}^{K,P} = \left(\sqrt{y_1}\mathbf{a}_1^{k,p}, \sqrt{y_1}\mathbf{a}_2^{k,p}, ..., \sqrt{y_1}\mathbf{a}_{x_1}^{k,p}, ..., \sqrt{y_c}\mathbf{a}_x^{k,p}\right) \tag{5}$$

$$\widetilde{B}^{K,P} = \left(\sqrt{x_1}\mathbf{b}_1^{k,p}, \sqrt{x_1}\mathbf{b}_2^{k,p}, ...\sqrt{x_1}\mathbf{b}_{y_1}^{k,p}, ..., \sqrt{x_c}\mathbf{b}_y^{k,p}\right) \tag{6}$$

$$M^{K,P} = \left(\sum_{D_{i=1}} \mathbf{a}_i^{k,p}, \sum_{D_{i=2}} \mathbf{a}_i^{k,p}, .., \sum_{D_{i=c}} \mathbf{a}_i^{k,p}\right) \tag{7}$$

$$F^{K,P} = \left(\sum_{H_{i=1}} \mathbf{b}_i^{k,p}, \sum_{H_{i=2}} \mathbf{b}_i^{k,p}, .., \sum_{H_{i=c}} \mathbf{b}_i^{k,p}\right) \tag{8}$$

$$n_I = \sum_{i=1}^{c} x_i \times y_i \tag{9}$$

In the above equations, $\mathbf{a}_i^{k,p}$ and $\mathbf{b}_i^{k,p}$ are the p^{th} column vectors of the k-mode flattening matrix A^k and B^k of the tensor samples $\boldsymbol{A}$ and $\boldsymbol{B}$, respectively. x_i and y_i are the number of samples in class i of $\boldsymbol{A}$ and $\boldsymbol{B}$, respectively. D_i and H_i are class labels.

$$\begin{aligned} n_E V_E^k &= \sum_{p=1}^{\prod_{o \neq k} I_o} n_E V_E^{k,P}, n_E V_E^{k,P} \\ &= y A^{K,P} \left(A^{K,P}\right)^T + x B^{K,P} \left(B^{K,P}\right)^T \\ &\quad - \mathbf{m}^{K,P} \left(\mathbf{f}^{K,P}\right)^T - \mathbf{f}^{K,P} \left(\mathbf{m}^{K,P}\right)^T - n_I V_I \end{aligned} \tag{10}$$

where

$$A^{K,P} = \left(\mathbf{a}_1^{K,P}, \mathbf{a}_2^{K,P}, .., \mathbf{a}_{x_1}^{K,P}, ..., \mathbf{a}_x^{K,P}\right) \tag{11}$$

$$B^{K,P} = \left(\mathbf{b}_1^{K,P}, \mathbf{b}_2^{K,P}, .., \mathbf{b}_{y_1}^{K,P}, ..., \mathbf{b}_y^{K,P}\right) \tag{12}$$

$$\mathbf{m}^{K,P} = \sum_{j=1}^{x} \mathbf{a}_i^{K,P} \tag{13}$$

$$\mathbf{f}^{K,P} = \sum_{j=1}^{y} \mathbf{b}_j^{K,P} \tag{14}$$

$$n_E = n_p \times n_c - n_I \tag{15}$$

where, n_p and n_c represent the number of parents and children, respectively. The optimization problem in (3) is a higher order nonlinear optimization problem with a higher order nonlinear constraint. Therefore, finding a straightforward closed solution is not clear. Hence, an iterative optimization approach to estimate the interrelated discriminative subspaces is proposed [39]. In each iteration U_K, K = 1,..., m are first initialized to identity. letting: $\boldsymbol{S} = \boldsymbol{A} \times_1 {U_1}^{itr-1} \cdots \times_{k-1} {U_{k-1}}^{itr-1} \times_{k+1} {U_{k+1}}^{itr-1} \cdots \times_m {U_m}^{itr-1}$ and $\boldsymbol{V} = \boldsymbol{B} \times_1 {U_1}^{itr-1} \cdots \times_{k-1} {U_{k-1}}^{itr-1} \times_{k+1} {U_{k+1}}^{itr-1} \cdots \times_m {U_m}^{itr-1}$ are substituted in (3) via changing $\boldsymbol{A}$ and $\boldsymbol{B}$ by $\boldsymbol{S}$ and $\boldsymbol{V}$.The new equation can be solved for each k-mode via eigenvectors decomposition as follows:

$$V_E^k U^k = \Lambda_k V_I^k U_k \tag{16}$$

where, U^k represents the eigenvectors matrix and Λ_k represents the eigenvalues matrix.

The Within-Class Covariance Normalization (WCCN) technique has been exploited for the first time by the community of speaker recognition, where Dehak et al. [6] demonstrated the utility of mapping the reduced vectors of LDA algorithm [33] to a novel subspace through the within-class covariance matrix. WCCN decreases the effect of the within class variations, thereby reducing the expected classification error in training data [1]. Here, we propose a variant of TXQDA which integrates WCCN as follows:

$$W_k = \sum_{j=1}^{C} \sum_{i=1}^{n_j} \left(U_T^k S_{j,i}^k - U_T^k \overline{S}_j^k\right) \left(U_T^k S_{j,i}^k - U_T^k \overline{S}_j^k\right)^T \tag{17}$$

where, U^k is the TXQDA projection matrix for each k-mode found in (16), $\overline{S}_j^k$ is the average matrix of class j samples. The WCCN projection matrix Z_k is obtained through Cholesky decomposition [11, 42] of the inverse of W_k as follow:

$$W_k^{-1} = Z_k Z_k^T \tag{18}$$

where our new projection matrix $U_k^{TXQDA_{WCCN}}$ is obtained by:

$$U_k^{TXQDA_{WCCN}} = Z_k^T U_k \tag{19}$$

The optimization of $\text{TXQDA}_{\text{WCCN}}$ method is performed iteratively and it breaks up on the achievement of one of the following conditions: i) the iterations number is reached or ii) $\left\| U_{\text{k}}^{\text{TXQDA}_{\text{WCCN}^{\text{itr}}}} - U_{\text{k}}^{\text{TXQDA}_{\text{WCCN}^{\text{itr-1}}}} \right\| < \text{I}_{\text{k}} \times \text{I}_{\text{k}} \times \epsilon$.

The entire procedure of the Tensor Cross-view Quadratic Discriminant Analysis integrating the within class covariance normalization $\text{TXQDA}_{\text{WCCN}}$ is provided in the algorithm 1.

Algorithm 1 $\text{TXQDA}_{\text{WCCN}}$.

Input:

- The tensor $\boldsymbol{A} \in \Re^{\text{I}_1 \times \text{I}_2 \cdots \times \text{I}_{\text{m}} \times \text{x}}$ comprises x training samples of the first view (Parents).
- The tensor $\boldsymbol{B} \in \Re^{\text{I}_1 \times \text{I}_2 \cdots \times \text{I}_{\text{m}} \times \text{y}}$ comprises y training samples of the second view (Children).
- The maximal number of iteration: $\text{itr}_{\max}$.
- The final lower dimensions: $\acute{\text{I}}_1 \times \acute{\text{I}}_2 \cdots \times \acute{\text{I}}_m$.

Output:

- The projection matrices of each mode $U_{\text{k}} = U_{\text{k}}^{\text{TXQDA}_{\text{WCCN}^{\text{itr}}}} \in \mathbb{R}^{\text{I}_{\text{k}}} \times \acute{\text{I}}_{\text{k}}$, $\text{k} = 1, \cdots, \text{m}$.

Algorithm:

1. **Initialization:** $U_1^0 = I_{\text{I}_1}, U_2^0 = I_{\text{I}_2}, \cdots, U_{\text{m}}^0 = I_{\text{I}_{\text{m}}}$
2. **For** itr : 1 to $\text{itr}_{\max}$
   (a) **For** k=1 to m
   - $\boldsymbol{S} = \boldsymbol{A} \times_1 U_1^{\text{itr}-1} \cdots \times_{\text{k}-1} U_{\text{k}-1}^{\text{itr}-1} \times_{\text{k}+1} U_{\text{k}+1}^{\text{itr}-1} \cdots \times_{\text{m}} U_{\text{m}}^{\text{itr}-1}$.
   - $S^{\text{k}} \Leftarrow {}_{\text{k}}\boldsymbol{S}$.
   - $\boldsymbol{V} = \boldsymbol{B} \times_1 U_1^{\text{itr}-1} \cdots \times_{\text{k}-1} U_{\text{k}-1}^{\text{itr}-1} \times_{\text{k}+1} U_{\text{k}+1}^{\text{itr}-1} \cdots \times_{\text{m}} U_{\text{m}}^{\text{itr}-1}$.
   - $V^{\text{k}} \Leftarrow {}_{\text{k}}\boldsymbol{V}$.
   - $\text{n}_{\text{I}} V_{\text{I}} = \sum_{\text{p}=1}^{\prod_{\text{o}\neq\text{k}}\text{I}_{\text{o}}} \text{n}_{\text{I}} V_{\text{I}}^{\text{P}}$, $\text{n}_{\text{I}} V_{\text{I}}^{\text{P}} = \widetilde{S}^{\text{K,P}} (\widetilde{S}^{\text{K,P}})^{\text{T}} + \widetilde{V}^{\text{K,P}} (\widetilde{V}^{\text{K,P}})^{\text{T}} - M^{\text{K,P}} (F^{\text{K,P}})^{\text{T}} - F^{\text{K,P}} (M^{\text{K,P}})^{\text{T}}$.
   - $\text{n}_{\text{E}} V_{\text{E}} = \sum_{\text{p}=1}^{\prod_{\text{o}\neq\text{k}}\text{I}_{\text{o}}} \text{n}_{\text{E}} V_{\text{E}}^{\text{P}}$, $\text{n}_{\text{E}} V_{\text{E}}^{\text{P}} = \text{y} S^{\text{K,P}} (S^{\text{K,P}})^{\text{T}} + \text{x} V^{\text{K,P}} (V^{\text{K,P}})^{\text{T}} - \mathbf{m}^{\text{K,P}} (\mathbf{f}^{\text{K,P}})^{\text{T}} - \mathbf{f}^{\text{K,P}} (\mathbf{m}^{\text{K,P}})^{\text{T}} - \text{n}_{\text{I}} V_{\text{I}}$.
   - Compute $V_{\text{E}}^{\text{k}} U_{\text{k}}^{\text{itr}} = \Lambda_{\text{k}} V_{\text{I}}^{\text{k}} U_{\text{k}}^{\text{itr}}$,obtain $U_{\text{k}}^{\text{itr}}$.
   - $W_{\text{k}} = \sum_{\text{j}=1}^{\text{C}} \sum_{\text{i}=1}^{\text{c}_{\text{j}}} (U_{\text{T}}^{\text{k}} S_{\text{j,i}}^{\text{k}} - U_{\text{T}}^{\text{k}} \overline{S}_{\text{j}}^{\text{k}})(U_{\text{T}}^{\text{k}} S_{\text{j,i}}^{\text{k}} - U_{\text{T}}^{\text{k}} \overline{S}_{\text{j}}^{\text{k}})^{\text{T}}$.
   - Compute WCCN projection matrix (Z_{k}) : $W_{\text{k}}^{-1} = Z_{\text{k}} Z_{\text{k}}^{\text{T}}$.
   - Compute the new projection matrix $U_{\text{k}}^{\text{TXQDA}_{\text{WCCN}^{\text{itr}}}}$: $U_{\text{k}}^{\text{TXQDA}_{\text{WCCN}^{\text{itr}}}} = Z_{\text{k}}^{\text{T}} U_{\text{k}}^{\text{itr}}$.

   (b) **If** itr >2 and $\left\| U_{\text{k}}^{\text{TXQDA}_{\text{WCCN}^{\text{itr}}}} - U_{\text{k}}^{\text{TXQDA}_{\text{WCCN}^{\text{itr-1}}}} \right\| < \text{I}_{\text{k}} \times \text{I}_{\text{k}} \times \epsilon$, $\text{k} = 1, \cdots, \text{m}$, break and go to step 3.
3. Sort the I_{m} eigenvectors $U_{\text{k}}^{\text{TXQDA}_{\text{WCCN}^{\text{itr}}}} \in \mathbb{R}^{\text{I}_{\text{k}} \times \text{I}_{\text{k}}}$ according to Λ_{k} in decreasing order, $\text{K} = 1, \cdots, \text{m}$.

2.3 Multilinear subspace transformation based on $\text{TXQDA}_{\text{WCCN}}$

In the training step, we create two 3rd order tensors $\boldsymbol{A}, \boldsymbol{B} \in \mathbb{R}^{\text{I}_1 \times \text{I}_2 \times \times \text{I}_3}$, $\boldsymbol{A}$ and $\boldsymbol{B}$ correspond to view 1 (Parents) and view 2 (Children), respectively. Each face image in the data sets is represented by a feature matrix as illustrated in Fig. 1. Mode-1 and Mode-2 of the training tensors correspond to rows and columns of this feature matrix, in which,

- Mode-1 is a feature vector resulted from one of each four descriptors mentioned previously (basic Gabor wavelets, hist-Gabor, LPQ+BSIf and VGG-Face).
- Mode-2 stores: different (scales + orientations) for basic Gabor wavelets and Hist-Gabor, multi descriptors for LPQ+BSIf, and different layers for VGG-Face.
- Mode-3 is employed to arrange the face samples in the dataset.

During the training phase, the optimal multilinear transformation matrices are estimated for each of tensor modes. In the test phase, the novel samples are projected using these transformation matrices before matching. The two training tensors $\boldsymbol{A}$ and $\boldsymbol{B}$ are projected in a new subspace based on $\text{TXQDA}_{\text{WCCN}}$. Consequently, the dimensions in each input tensors are reduced according to I_1 and I_2

modes; the third dimension I_3 remains the same because it represents the samples of the database. Therefore, new reduced and discriminative tensors are obtained, where $\acute{I}_1 \times \acute{I}_2 << I_1 \times I_2$. The test images passes through the similar stages as in the training phase. Firstly, the feature extraction is performed, after that, the test faces are projected into a new multilinear subspace based on $\text{TXQDA}_{\text{WCCN}}$. Finally, the cosine similarity [30] is used to examine whether the pair belonging to the same family or not (kin or not-kin). The cosine similarity of two feature vectors $\mathbf{v}_{t_1}$ and $\mathbf{v}_{t_2}$ in the $\text{TXQDA}_{\text{WCCN}}$ subspace is defined as follows:

$$a_i = \cos(\mathbf{v}_{t_1}, \mathbf{v}_{t_2}) = \frac{\mathbf{v}_{t_1}^{T}.\mathbf{v}_{t_2}}{\|\mathbf{v}_{t_1}\|.\|\mathbf{v}_{t_2}\|} \tag{20}$$

2.4 Logistic regression based score level fusion

We adopt a score-level fusion strategy to take advantage of combining the similarity scores exploiting the complementarity of the two feature types aiming to increase the accuracies. For this purpose, Logistic Regression (LR) [10] is used in our framework. We select the logistic regression method because it has achieved interesting fusion improvements. The LR performs a simple decision based on an hyperplane and it converges around a global optimal solution. By taking the scores a_i as the input, the generated probability (output) b_i is defined as follow:

$$b_i = (1 + \exp(xa_i + y))^{-1} \tag{21}$$

where x is a scalar factor and y is a bias.

3 Experiments

In order to evaluate and assess the effectiveness of our approach, in this section, we conduct several experiments on three benchmark kinship datasets, namely Cornell Kinface, UB KinFace and TSKinface. In the following, we first introduce the three datasets used in our experiments. Then, we present the experimental protocol and parameters settings and detail the experimental results with their analysis. The performances of the proposed approach are evaluated separately based on VGG-Face, (LPQ+BSIf), basic Gabor, Hist-Gabor as well as their combinations via LR score fusion. Finally, our best results are compared with the state of art.

3.1 Datasets

- **Cornell KinFace database** [8] contains 150 parent-child face image pairs, encompassing the four kinship relations. These face images are collected from the web. Due to privacy issues, seven families (parent–child pairs) have been taken out from the dataset. Thus, there are totally 286 RGB cropped face images with size 100×100 pixels.
- **UB KinFace database** [36] contains 600 images of 400 unique subjects, divided into 200 groups of child-young parent (set 1) and 200 groups of child-old parent (set 2). Most of face images in the database are true-world combinations collected from the internet. It is considered as the first dataset, which takes a new view of kinship verification problem (young and old face images of parents).
- **TSKinFace database** [35] is among the biggest existing kinship databases. It contains 4060 face images with two kinds of three subject kinship relations: Father-Mother-Son (FM-S) and Father-Mother-Daughter (FM-D). The FM-S comprises 513 relations and FM-D has 502 relations. Since we deal with pair matching, we reorganized the database by splitting the group of FM-S into two subsets Father-Son (F-S) and Mother-Son (M-S) relations and the group of FM-D into two subsets Father-Daughter (F-D) and Mother-Daughter (M-D) relations.

3.2 Experimental protocol

For a fair the evaluation of our method, we follow the same protocol as the stat of the art [28, 37, 38], in which five folds with cross-validation strategy is used. This protocol is adopted to ensure that our results are straightforwardly comparable to the previous works in kinship verification. Each fold contains almost a similar number of face pairs. The positive pairs are predefined by the dataset collectors while the negative pairs generated via combination of a parent image and are randomly selected image from the set of children images from which the current parent's children images are omitted.

3.3 Parameters settings

All the face images are aligned then cropped into 126×115 pixels, 96×89 pixels and 64×64 pixels for Cornell KinFace, UB KinFace and TSKinface datasets, respectively. The face images corresponding to each pair are processed according to our proposed kinship verification scheme in order to extract the handcrafted and deep features. For the description of face image, four types of features with different parameters are extracted:

- Hist-Gabor: To optimize our new descriptor, we have tested several combinations among the responses of 40 Gabor filters. We found the magnitude at 2 frequencies ($v = 8, 8\sqrt{2}$) and 3 orientations ($\theta = \pi/8, \pi/4, 3\pi/8$) to perform enough well. As described in Section 2.1.1, we apply these 6 Gabor filters on the face image and each resulting image is divided into 14 blocks whose

Table 2 The verification accuracies (%) of TXQDA and $TXQDA_{WCCN}$ using different features and their fusion on TSKinFace database

Type of Features	TXQDA					**$TXQDA_{WCCN}$**				
	FS	FD	MS	MD	Mean	FS	FD	MS	MD	Mean
Basic Gabor	65.05	64.06	63.30	62.60	63.75	70.00	68.51	72.14	69.94	70.15
Hist-Gabor	84.85	85.45	84.56	85.91	85.19	91.17	89.80	89.71	89.78	90.12
(LPQ+BSIf)	87.86	87.72	88.45	87.99	88.00	91.36	92.48	92.82	92.76	92.35
VGG-Face	71.07	71.98	71.46	73.01	71.88	77.38	78.12	79.32	80.06	78.72
Hist-Gabor+(LPQ+BSIf)	90.58	90.79	90.58	90.47	90.60	93.11	92.48	93.40	92.86	92.96
Hist-Gabor+VGG-Face	86.70	87.33	86.02	86.71	86.69	92.52	91.58	92.72	91.27	92.02
(LPQ+BSIf)+VGG-Face	87.77	87.82	88.25	87.98	91.75	92.48	92.80	93.05	92.52	88.09
Basic Gabor+(LPQ+BSIf)+VGG-Face	87.67	88.12	88.06	88.79	88.16	91.65	92.08	92.82	93.16	92.43
Hist_Gabor+(LPQ+BSIf)+VGG-Face	90.78	90.89	90.68	90.47	90.70	93.50	93.47	93.79	93.55	93.58

histograms are concatenated in a feature vector. The vectors of the six components construct a feature matrix of dimension 4096×6.

- Basic Gabor: For fair comparison, we keep the same parameters as Hist-Gabor but without the subdivision of the images and without computing the histograms. Instead, each component is vectorized to get one feature vector. Then, all feature vectors are concatenated to get a feature matrix of dimension $d \times 6$, where d is the number of the image pixels.
- LPQ+BSIf: For handcrafted features, we extract one scale for each descriptor, LPQ with a window of size M=3 and BSIf with learnt filters of size l=5, and divide each face image into 24 blocks. Then, each of the 24 blocks is summarized into a histogram of 256 bins and the histograms are concatenated in a feature vector of size 6144. We employ the two feature vectors, resulting from LPQ and BSIf, to build a feature matrix of dimension 6144×2.
- VGG-Face: as deep features, we extract the features from the face image of size $224 \times 224 \times 3$ using 4 layers of VGG-Face network: fc6, relu6, fc7 and relu7. The four vectors construct a feature matrix of dimension 4096×4.

3.4 Results and discussion

The evaluation results of the proposed TXQDA and $TXQDA_{WCCN}$ using single features and the LR fusion of their combinations are shown in Tables 2, 3 and 4 for the three benchmark kinship datasets. These results outline four principal observations which are detailed in the following.

3.4.1 The proposed Hist-Gabor outperforms the basic Gabor

We can observe a significant weakness in the discrimination power of the basic Gabor method compared with the proposed Hist-Gabor on the three databases. To be specific, compared to the basic Gabor, the proposed Hist-Gabor attains an accuracy improvement of 19.70%, 33.34% and 29.48% on TSKinFace, Cornell KinFace and UB kinface datasets, respectively (see Tables 2 to 4). These results

Table 3 The verification accuracies (%) of TXQDA and $TXQDA_{WCCN}$ using different features and their fusion on the UB KinFace database

Type of Features	TXQDA			**$TXQDA_{WCCN}$**		
	Set1	Set2	Mean	Set1	Set2	Mean
Basic Gabor	56.28	55.36	55.82	58.48	60.53	59.50
Hist-Gabor	87.45	88.25	87.85	88.45	89.52	88.98
(LPQ+BSIf)	86.90	87.47	87.18	88.20	89.51	88.85
VGG-Face	87.86	85.43	86.64	88.39	86.21	87.30
Hist-Gabor+(LPQ+BSIf)	89.92	90.78	90.35	89.18	91.02	90.10
Hist-Gabor+VGG-Face	89.85	90.24	90.04	90.90	91.76	91.33
(LPQ+BSIf)+VGG-Face	89.36	90.70	90.03	90.65	91.23	90.94
Basic Gabor+(LPQ+BSIf)+VGG-Face	89.37	91.23	90.30	90.67	92.25	91.46
Hist_Gabor+(LPQ+BSIf)+VGG-Face	90.61	92.73	91.67	90.91	92.76	91.83

Table 4 The verification accuracies (%) of TXQDA and $TXQDA_{WCCN}$ using different features, and their fusion on the Cornell KinFace database

Type of Features	TXQDA Mean	$\mathbf{TXQDA_{WCCN}}$ Mean
Basic Gabor	55.23	57.62
Hist-Gabor	89.24	90.96
(LPQ+BSIf)	91.33	92.37
VGG-Face	89.62	91.02
Hist-Gabor+(LPQ+BSIf)	92.43	92.72
Hist-Gabor+VGG-Face	93.46	94.18
(LPQ+BSIf)+VGG-Face	93.39	94.41
Basic Gabor+(LPQ+BSIf)+VGG-Face	93.41	94.81
Hist_Gabor+(LPQ+BSIf)+VGG-Face	94.87	95.14

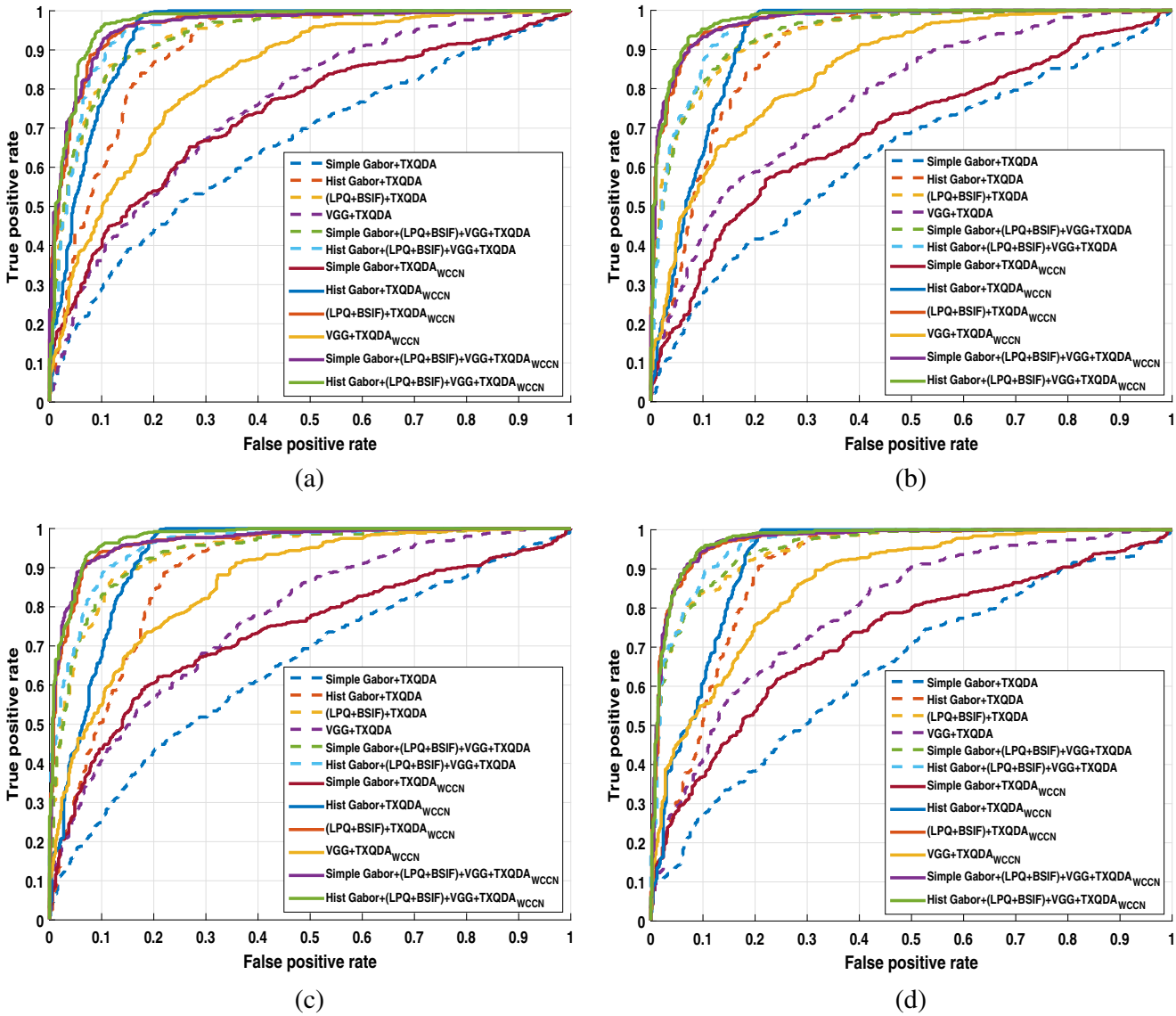

Fig. 4 ROC curves of TXQDA vs.$TXQDA_{WCCN}$ using different features and their fusion on TSKinFace. **a** F-S set, **b** F-D set, **c** M-S set and **d** M-D set

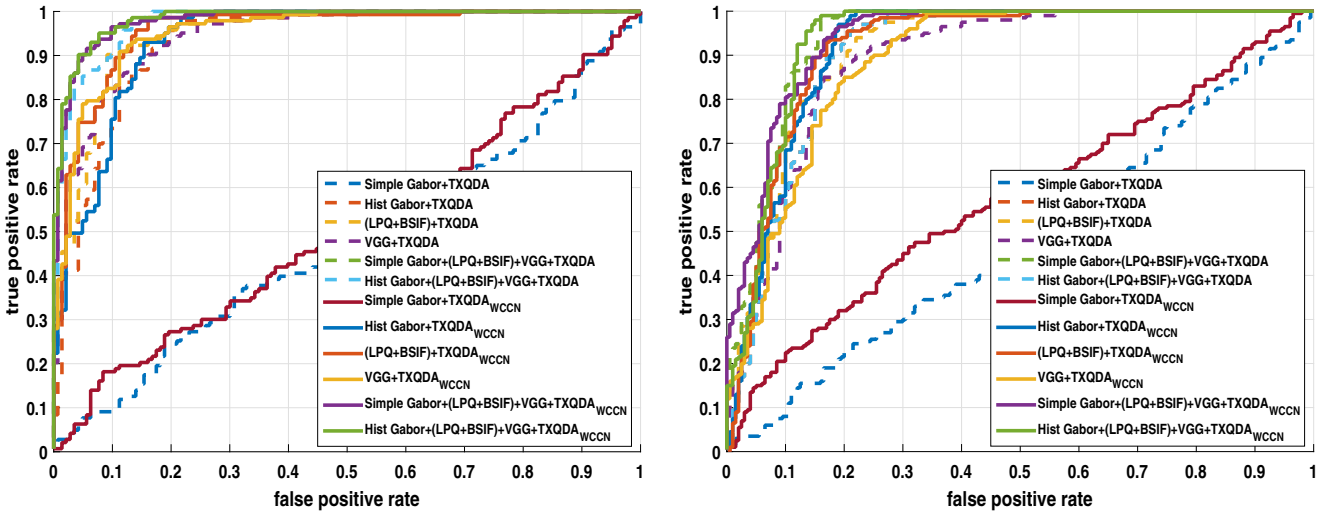

Fig. 5 ROC curves of TXQDA vs.TXQDA$_{WCCN}$ using different features and their fusion on **a** Cornell KinFace **b** UB KinFace set 2

confirm the utility of dividing the face image into a several blocks and taking their histograms as a discriminative biometric signature.

3.4.2 WCCN improves the TXQDA performances

By comparing the results depicted in the Tables 2, 3 and 4, we can note that the proposed TXQDA$_{WCCN}$ outperforms TXQDA on the three databases. Thanks to WCCN, the within-class variations effect is decreased thereby reducing the predictable classification error. Indeed, the proposed TXQDA$_{WCCN}$ maps the extracted features into a discriminative subspace and providing more discrimination power and robustness to the features to be used in the comparison step. In our case, overall, TXQDA$_{WCCN}$ improves the accuracy of the basic TXQDA with a percentage of 2-5%.

3.4.3 LR fusion enhances the results of single features

For a better visualization and easier comparison of different experimental configurations, the Receiving Operating Characteristic (ROC) Curves of different methods are plotted in Figs. 4 for the four relation of TSKinFace and in 5 for Cornell and UB kinface databases. We can observe from these figures that LR fusion yields competitive performances than using each type of features alone in terms of ROC curves. This result is attributed to the fact that every feature contributes efficiently to the kinship verification system and the fusion of these contributions further improves the performances. It is worth noting that when we fuse the scores resulting from the three types of features (VGG-Face, Hist-Gabor and LPQ+BSIf), the LR fusion process reaches a high performance of 93.58%, 95.14% and 92.17% on the UB kinface, Cornell Kinface and TSKinFace databases, respectively.

3.4.4 VGG-Face features provide weak accuracies on small databases

From our results (see Tables 2 and 4), we notice a relative weakness in the effectiveness of the VGG-Face features as in most of the cases they yield lower accuracies. Indeed, it is often realized that the deep CNN does not perform very well on small datasets such as those used in kinship verification. This result confirms the conclusion drawn by a previous work [44].

3.5 Evaluation of time complexity

To estimate the computational complexity of the proposed TXQDA$_{WCCN}$ for practical applications, we compute the CPU time needed to execute the algorithm for matching one pair of face image in the online stage. The utilized hardware configuration comprises an Intel Xeon(R) 3.19 GHz CPU and a 12 GB of RAM using Matlab R2018a. Table 5 lists the CPU time (in milliseconds) of our algorithm on all three evaluation databases. We see that the computational time for

Table 5 Running time of the proposed algorithm on the three datasets

Dataset	CPU time
TSKinFace	4.97
UB KinFace	5.49
Cornell KinFace	6.09

Table 6 Comparison to state of the art on TSKinFace database

Approach type	Author	Year	Mean Accuracy (%)
Metric learning	Lu et al. [27]	2017	84.15
	Liang et al. [22]	2018	90.47
	Laiadi et al. [18]	2018	83.63
Multi metric learning	Laiadi et al. [16]	2019	88.59
	Bessaoudi et al. [3]	2019	85.18
Multilinear subspace learning	Laiadi et al. [17]	2020	90.32
	Proposed	2020	90.70

Table 7 Comparison to state of the art on UB KinFace database

Approach type	Author	Year	Mean Accuracy (%)
Metric Learning	Lu et al. [28]	2014	65.60
	Zhou al. [45]	2018	75.50
Multi Metric Learning	Lu et al. [28]	2014	67.05
	Yan et al. [38]	2014	72.25
	Bessaoudi et al. [3]	2019	83.34
Multilinear subspace learning	Laiadi et al. [17]	2020	91.53
	Proposed	2020	91.83

Table 8 Comparison to state of the art on Cornell KinFace database

Approach type	Author	Year	Mean Accuracy (%)
Metric learning	Lu et al. [28]	2014	69.50
	Zhou al. [45]	2018	81.40
	Laiadi et al. [18]	2018	77.60
Multi metric learning	Lu et al. [28]	2014	71.60
	Yan et al. [38]	2014	73.50
	Mahpod et Keller [29]	2017	76.60
	Bessaoudi et al. [3]	2019	86.87
Multilinear subspace learning	Laiadi et al. [17]	2020	93.04
	Proposed	2020	95.14

Table 9 Increase in average accuracy provided by $\text{TXQDA}_{\text{WCCN}}$ compared to the state of the art

Approach type	Database	Best method	Increase in average accuracy (%)
Metric learning	Cornell KinFace	Zhou al. [45]	13.74
	TSKinFace	Liang et al. [22]	0.23
	UB KinFace	Zhou al. [45]	16.33
Multi metric learning	Cornell KinFace	Laiadi et al. [18]	18.54
	TSKinFace	Laiadi et al. [16]	02.11
	UB KinFace	Yan et al. [38]	19.58
Multilinear subspace learning	Cornell KinFace	Laiadi et al. [17]	2.10
	TSKinFace	Laiadi et al. [17]	0.40
	UB KinFace	Laiadi et al. [17]	0.30

our approach using Hist Gabor+(LPQ+BSIf)+VGG-Face features is around 4.97 ms for TSKinFace, 5.49 ms for UB KinFace, and 6.09 ms for Cornell KinFace database. These experimental results confirm that the required verification time is only few milliseconds. Hence, demonstrating the feasibility and success of using our approach for real time face kinship verification applications.

3.6 Comparison to the state of the art

The best performance of the proposed method $\text{TXQDA}_{\text{WCCN}}$ with score fusion of Hist-Gabor, (LPQ+BSIf) and VGG-Face is compared with recent related works in Table 6 on TSKinFace database, in Table 7 on UB KinFace and in Table 8 on Cornell KinFace database. For comparison purpose, the recent related works, grouped according to three categories, metric, multi-metric and multilinear learning approaches, are reported. This comparison demonstrates that the proposed approach outperforms the state of the art on the three databases. Table 9 shows the increase in average accuracy provided by our method compared to the best method of each category. This table demonstrates the effectiveness of our method for kinship verification task.

It is worth noting that we were able to considerably improve the kinship verification accuracy on the UB Kinface database. This database is considered as one of the hardest kinship verification databases. This is due to the fact that the pairs of face images of this database are not cropped from the same image, this means that the face pair images are not captured under the same environment. In the literature, the best kinship verification accuracy on this database does not exceed 90%. Whereas, our proposed approach achieved an accuracy of 92.17% resulting from the LR scores fusion of the Hist-Gabor, (LPQ+BSIf) and VGG-Face features.

4 Conclusion

In this paper, we presented an efficient approach for face based kinship verification using handcrafted and deep tensor features. Besides exploiting two state-of-the-art face descriptors, we introduced a new face descriptor, Hist-Gabor, based on the Gabor wavelets responses. To enhance the discrimination of the proposed multidimensional face representations, we have proposed $\text{TXQDA}_{\text{WCCN}}$ as a multilinear subspace learning method. $\text{TXQDA}_{\text{WCCN}}$ finds multiple interrelated projection matrices for mapping high order tensor data through exploiting combined traits of multi-view representation. This allows minimizing the variation of the within-class while maximizing the variation of the between-class from all views at the same time.

The proposed Hist-Gabor achieves interesting performances compared with its counterpart basic Gabor method. The best performances of our approach are achieved by fusing the scores of the handcrafted and the deep tensor features using LR technique. Hence, our results confirm that handcrafted and deep features are complementary and their fusion greatly helps increasing the verification of kin relations accuracy. Moreover, the experimental part confirms that our approach $\text{TXQDA}_{\text{WCCN}}$ exhibits superior results over recently reported kinship verification methods on three challenging datasets. In future, we plan to enhance our method so that it able to handle the supervised and semi supervised scenarios in other face verification applications.

References

1. Barkan O, Weill J, Wolf L, Aronowitz H (2013) Fast high dimensional vector multiplication face recognition. In: Proceedings of the IEEE international conference on computer vision, pp. 1960–1967
2. Bessaoudi M, Belahcene M, Ouamane A, Chouchane A, Bourennane S (2019) Multilinear enhanced fisher discriminant analysis for robust multimodal 2d and 3d face verification. Appl Intell 49(4):1339–1354
3. Bessaoudi M, Ouamane A, Belahcene M, Chouchane A, Boutellaa E, Bourennane S (2019) Multilinear side-information based discriminant analysis for face and kinship verification in the wild. Neurocomputing 329:267–278
4. Boutellaa E, López MB, Ait-Aoudia S, Feng X, Hadid A (2017) Kinship verification from videos using spatio-temporal texture features and deep learning
5. Dal Martello MF, Maloney LT (2006) Where are kin recognition signals in the human face? J Vis 6(12):2–2
6. Dehak N, Kenny PJ, Dehak R, Dumouchel P, Ouellet P (2010) Front-end factor analysis for speaker verification. IEEE Transactions on Audio Speech, and Language Processing 19(4):788–798
7. Fang L, Li S (2015) Face recognition by exploiting local gabor features with multitask adaptive sparse representation. IEEE Trans Instrum Meas 64(10):2605–2615
8. Fang R, Tang KD, Snavely N, Chen T (2010) Towards computational models of kinship verification. In: 2010 IEEE International conference on image processing, pp. 1577–1580. IEEE
9. Guo G, Wang X (2012) Kinship measurement on salient facial features. IEEE Trans Instrum Meas 61(8):2322–2325
10. Harrell Jr FE (2015) Regression modeling strategies: with applications to linear models, logistic and ordinal regression, and survival analysis Springer
11. Iman RL, Conover WJ (1982) A distribution-free approach to inducing rank correlation among input variables. Communications in Statistics-Simulation and Computation 11(3):311–334
12. Kaminski G, Dridi S, Graff C, Gentaz E (2009) Human ability to detect kinship in strangerb faces: effects of the degree of relatedness. Proc R Soc B Biol Sci 276(1670):3193–3200
13. Kaminski G, Ravary F, Graff C, Gentaz E (2010) Firstborns' disadvantage in kinship detection. Psychological science 21(12):1746–1750
14. Kannala J, Rahtu E (2012) Bsif: Binarized statistical image features. In: Proceedings of the 21st international conference on pattern recognition (ICPR2012), pp. 1363–1366. IEEE

15. Kofman A (2016) The troubling rise of rapid dna testing. goo gl/uuhZSN
16. Laiadi O, Ouamane A, Benakcha A, Taleb-Ahmed A, Hadid A (2019) Learning multi-view deep and shallow features through new discriminative subspace for bi-subject and tri-subject kinship verification. Appl Intell 49(11):3894–3908
17. Laiadi O, Ouamane A, Benakcha A, Taleb-Ahmed A, Hadid A (2020) Tensor cross-view quadratic discriminant analysis for kinship verification in the wild. Neurocomputing 377:286–300
18. Laiadi O, Ouamane A, Boutellaa E, Benakcha A, Taleb-Ahmed A, Hadid A (2019) Kinship verification from face images in discriminative subspaces of color components. Multimedia Tools and Applications 78(12):16465–16487
19. Lee TS (1996) Image representation using 2d gabor wavelets. IEEE Transactions on pattern analysis and machine intelligence 18(10):959–971
20. Li C, Huang Y, Xue Y (2019) Dependence structure of gabor wavelets based on copula for face recognition. Expert Syst Appl 137:453–470
21. Li W, Wu Y, Li J (2017) Re-identification by neighborhood structure metric learning. Pattern Recogn 61:327–338
22. Liang J, Hu Q, Dang C, Zuo W (2018) Weighted graph embedding-based metric learning for kinship verification. IEEE Trans Image Process 28(3):1149–1162
23. Liao S, Hu Y, Zhu X, Li SZ (2015) Person re-identification by local maximal occurrence representation and metric learning. In: Proceedings of the IEEE conference on computer vision and pattern recognition, pp. 2197–2206
24. Liong VE, Lu J, Ge Y (2015) Regularized local metric learning for person re-identification. Pattern Recogn Lett 68:288–296
25. Lu H, Plataniotis KN, Venetsanopoulos AN (2008) Mpca: Multilinear principal component analysis of tensor objects. IEEE transactions on Neural Networks 19(1):18–39
26. Lu H, Plataniotis KN, Venetsanopoulos AN (2008) Uncorrelated multilinear discriminant analysis with regularization and aggregation for tensor object recognition. IEEE Transactions on Neural Networks 20(1):103–123
27. Lu J, Hu J, Tan YP (2017) Discriminative deep metric learning for face and kinship verification. IEEE Trans Image Process 26(9):4269–4282
28. Lu J, Zhou X, Tan YP, Shang Y, Zhou J (2013) Neighborhood repulsed metric learning for kinship verification. IEEE transactions on pattern analysis and machine intelligence 36(2):331–345
29. Mahpod S, Keller Y (2018) Kinship verification using multiview hybrid distance learning. Comput Vis Image Underst 167:28–36
30. Nguyen HV, Bai L (2010) Cosine similarity metric learning for face verification. In: Asian conference on computer vision, pp. 709–720. Springer
31. Ojansivu V, Heikkilä J. (2008) Blur insensitive texture classification using local phase quantization. In: International conference on image and signal processing, pp. 236–243. Springer
32. Ouamane A, Chouchane A, Boutellaa E, Belahcene M, Bourennane S, Hadid A (2017) Efficient tensor-based 2d+ 3d face verification. IEEE Transactions on Information Forensics and Security 12(11):2751–2762
33. Pang Y, Wang S, Yuan Y (2014) Learning regularized lda by clustering. IEEE transactions on neural networks and learning systems 25(12):2191–2201
34. Parkhi OM, Vedaldi A, Zisserman A (2015) Deep face recognition. In: British machine vision conference
35. Qin X, Tan X, Chen S (2015) Tri-subject kinship verification: Understanding the core of a family. IEEE Transactions on Multimedia 17(10):1855–1867
36. Xia S, Shao M, Luo J, Fu Y (2012) Understanding kin relationships in a photo. IEEE Transactions on Multimedia 14(4):1046–1056
37. Yan H (2017) Kinship verification using neighborhood repulsed correlation metric learning. Image Vis Comput 60:91–97
38. Yan H, Lu J, Deng W, Zhou X (2014) Discriminative multimetric learning for kinship verification. IEEE Transactions on Information forensics and security 9(7):1169–1178
39. Yan S, Xu D, Yang Q, Zhang L, Tang X, Zhang HJ (2006) Multilinear discriminant analysis for face recognition. IEEE Trans Image Process 16(1):212–220
40. Yang D, Jiao L, Gong M, Liu F (2011) Artificial immune multiobjective sar image segmentation with fused complementary features. Inf Sci 181(13):2797–2812
41. Yang Y, Sun J (2010) Face recognition based on gabor feature extraction and fractal coding. In: 2010 Third international symposium on electronic commerce and security, pp. 302–306. IEEE
42. Yu H, Chung C, Wong K, Lee H, Zhang J (2009) Probabilistic load flow evaluation with hybrid latin hypercube sampling and cholesky decomposition. IEEE Transactions on Power Systems 24(2):661–667
43. Yuan S, Mao X, Chen L (2017) Multilinear spatial discriminant analysis for dimensionality reduction. IEEE Trans Image Process 26(6):2669–2681
44. Zhang L, Duan Q, Zhang D, Jia W, Wang x. (2020) Advkin: Adversarial convolutional network for kinship verification. IEEE Transactions on Cybernetics
45. Zhou X, Jin K, Xu M, Guo G (2019) Learning deep compact similarity metric for kinship verification from face images. Information Fusion 48:84–94
46. Zhou X, Lu J, Hu J, Shang Y (2012) Gabor-based gradient orientation pyramid for kinship verification under uncontrolled environments. In: Proceedings of the 20th ACM international conference on Multimedia, pp. 725–728

Mohcene Bessaoudi Received the Ph.D degree in Electronic Telecommunication from University of Mohammed Khider Biskra, Algeria in 2019 at the Department of Electrical Engineering. His research interests are in: image processing, feature extraction, face detection, tensor analysis, classification, computer vision, biometric techniques and face recognition systems.

Ammar Chouchane Received the Ph.D degree in Electronic Telecommunication from University of Mohammed Khider Biskra, Algeria in 2016. Currently, he is a Lecturer at Electrical Engineering Department at university of Yahia Fares Medea, Algeria. His research interests are in image processing, feature extraction, face detection, tensor analysis, classification, computer vision, biometric techniques and face recognition systems.

Abdelmalik Ouamane Received the Doctor of Science degree from University of Mohammed Khider Biskra, Algeria in 2015. Currently, he is a Lecturer at Electrical Engineering Department at the same university. He has been a reviewer for many conferences and journals. His research interests include image processing, classification, multimodal biometric and tensor analysis.

Elhocine Boutellaa Received Ph.D. degree in Computer Science from Ecole Nationale Supérieure d'Informatique, Algeria. He has been working as research associate with Centre de Développement des Technologies Avancées since 2010. Currently he holds the position of postdoctoral researcher at Centre de Développment Technologie Avancés, Algiers, Algeria. His research interests include face analysis, biometrics and computer vision.